**NURETH14-361** 

# BENCHMARK ANALYSES OF SODIUM CONVECTION IN THE UPPER PLENUM OF THE MONJU REACTOR VESSSEL

- Comparison between plant system analysis code CERES and CFD code -

Y. Nishi<sup>1</sup>, N. Ueda<sup>1</sup>, S. Yoshikawa<sup>2</sup>, A. Miyakawa<sup>2</sup> and M. Kato<sup>3</sup>

<sup>1</sup> Central Research Institute of Electric Power Industry (CRIEPI), Tokyo, Japan

<sup>2</sup> Japan Atomic Energy Agency (JAEA), <sup>3</sup>NESI Inc., Fukui, Japan

#### Abstract

In the CRP of IAEA, the data of the upper plenum geometry of the prototype FBR"MONJU" and the boundary conditions of the plant trip test were provided by JAEA. A plant system analysis code CERES for FBRs was developed by CRIEPI. To verify the CERES code, analyses had been performed for the system test of the MONJU, the results of which showed good agreement with the test. However, the difficulty of accurately reproducing the temperature variation arising from a complex flow in the upper plenum was identified. By using the general-purpose analysis code STAR-CCM+, detailed analysis in the upper plenum was enabled. Based on comparison between analyses of the CERES and STAR-CCM+ codes, parameters that had to be considered to simulate the flow pattern appropriately for plant system analysis codes were discussed. And, the analysis capability of CERES code with appropriate parameter was able to be confirmed.

#### Introduction

CERES is a plant system analysis code for LMRs (liquid metal cooled reactors) In conventional system analysis code, cooling system are modeled one-dimensionally, and connected to the flow network [1]. However, the effect of multidimensional flow in plant dynamics may not be negligible in components with a large plenum such as Reactor Vessel (R/V). The effect becomes significant, particularly when the flow-field is a complex condition. Normally, a special three dimensional thermal-hydraulic analysis code (CFD code) has been applied to evaluate such complex flow under the boundary conditions obtained from the results of other flow network calculations. However, the calculation had to be repeated through the boundary conditions between the CFD and flow network codes when evaluating the transition of the plant characteristics.

CERES has the function of calculating the multidimensional coolant flow in the plena in addition to the one-dimensional flow network calculation [2]. In the construction of the CERES code, the lightness, handling and a suitable multi-dimensional analytical function as the flow network code were considered, meaning a very simple model is employed in multi-dimensional function compared with a modern CFD code [3]. To verify the CERES code, analyses were performed for the system test of the MONJU, the results of which showed good agreement with the test. However, the difficulty of accurately reproducing the temperature variation arising from a complex flow in the upper plenum was identified.

In the Coordinated Research Project (CRP) of IAEA, the data of the upper plenum geometry and the boundary conditions are provided by JAEA. By using a CFD code STAR-CCM+ ver. 4.04.011, a detailed calculation was performed with those data. To obtain beneficial information for the flow network model, a comparison between the analyses of the CERES and STAR-CCM+ codes was performed.

# 1. The configuration of the MONJU upper plenum

The plant trip test of the "MONJU" was carried out in December 1995. Figure 1 and 2 show an image of the primary main cooling system. The pony motor operation is started when the primary main circulation pump is tripped by the plant tripping and the primary system is operated steadily at approx. 10 % of the rated flow rate. The temperature distribution in the axial direction of the R/V upper plenum was measured by a temporarily installed thermo-couple tree as shown in Figs. 3 and 4. High temperature sodium from the core rises up in the space inside the inner barrel, turns to an annular space between the inner barrel and the R/V, and flows to the IHX through the R/V outlet nozzle. Flow holes exist on two elevations of the inner barrel as shown in Fig. 4. The sodium also flows out from these holes to the annular space.

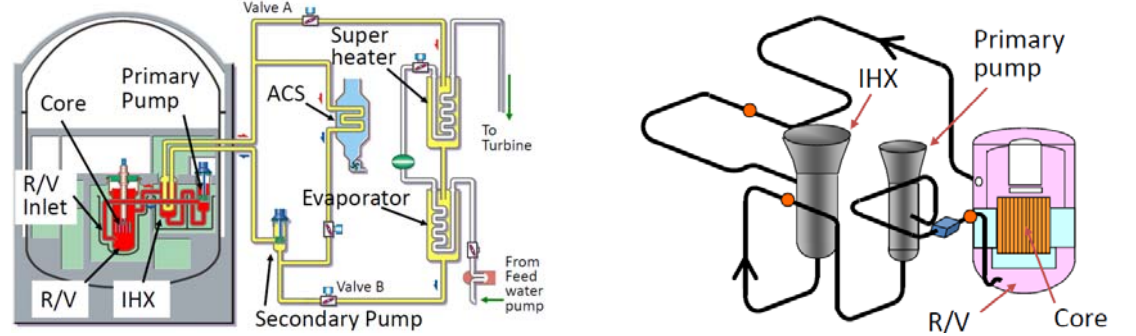


Fig. 1 Cooling system of the MONJU

Fig. 2 Primary main cooling system (Red circle: TC)

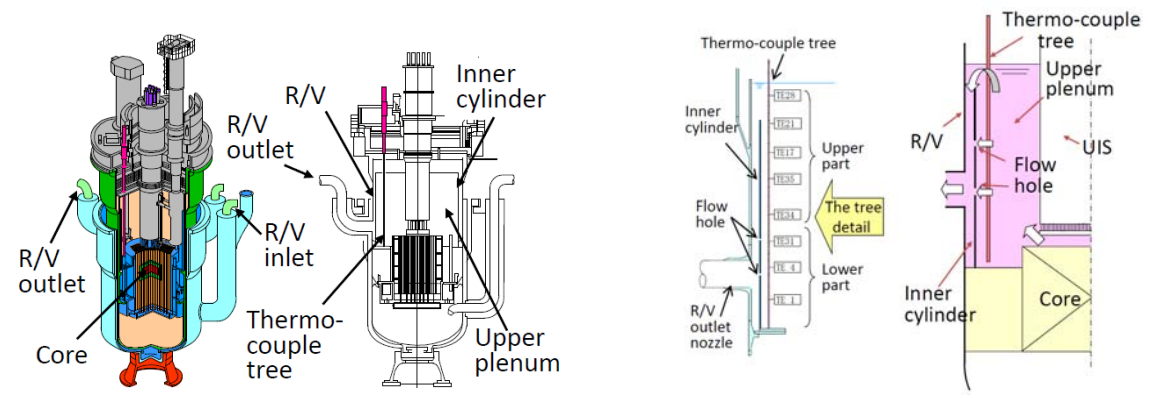


Fig. 3 Schematic diagram of the R/V

Fig. 4 Schematic diagram of the upper plenum

## 2. CERES modeling and boundary conditions

Figure 5 shows the mesh partition used in the CERES code during this analysis. MONJU has three heat transfer circuits (known as "A", "B" and "C" loops), and the volume for a circuit is modeled by employing a 1/3 (120°) sector model. Using a cylindrical coordinate system, the mesh partition is 41 in the R-direction, 148 in the Z-direction and 7 in the  $\theta$  (perimeter) direction, with the total number of meshes 42476. Inlet and outlet nozzles are located at positions of k=3 and k=5 in the  $\theta$ -direction, respectively. The piping model is joined to the upstream portion of the R/V inlet nozzle, while the inlet boundary is located at the pipe terminal. The terminal is in the same position as the R/V inlet thermocouple shown in Fig. 2 (red closed circle)[4]. A free slip condition is applied to the wall surface and the periodic boundary condition to the  $\theta$ -direction for calculation. In the CRP, data of the outlet temperature and the flow rate of each subassembly were provided as boundary conditions, while the simulation of the sodium flow pattern and the temperature distribution in the upper plenum were only evaluated. On the other hand, the R/V inlet temperature and flow rate, as shown in Figs. 6 and 7 respectively[5], had the CERES calculation applied. The plenum hydraulic model is as follows; Non-compression viscous flow models of two or three dimensions. Volume porosity and surface permeability are utilized to evaluate the plenum shape and the volume accurately[5].

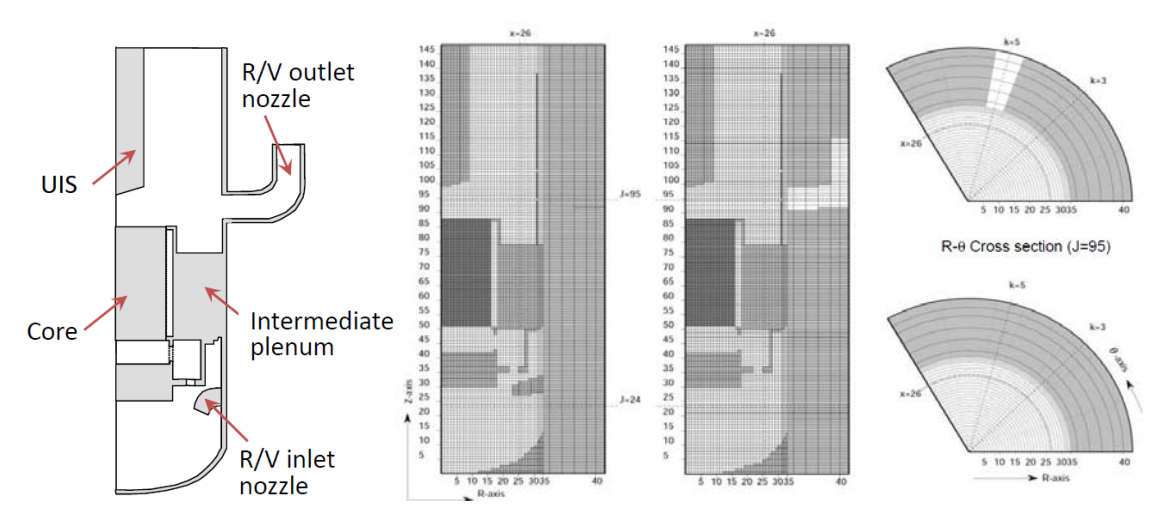
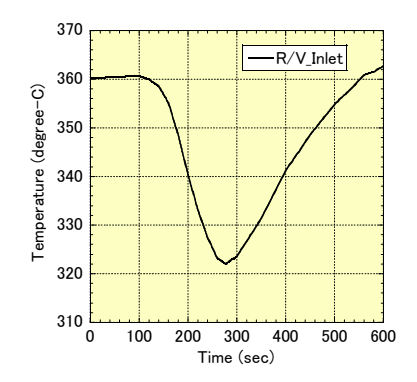


Fig. 5 CERES model and mesh division



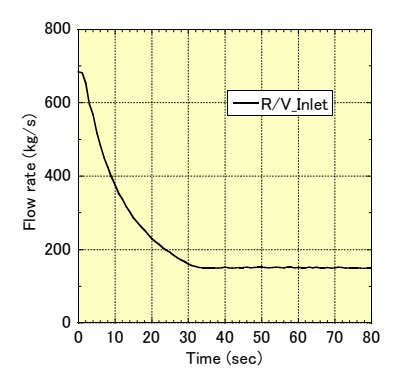


Fig. 6 Inlet boundary condition (Temperature)[5] Fig. 7 Inlet boundary condition (flow rate)[5]

Multiple round holes are provided at two heights of the inner barrel (Fig. 4), which are simulated in terms of permeability and mesh porosity at the boundary of the node. The pressure loss coefficient of the flow hole is set to 0.8, which is a proposal derived by the data optimization work with the Super-COPD [4].

# 3. STAR-CCM+ modeling and boundary conditions

Figure 8 shows the geometry for the STAR-CCM+ calculation, for which the 1/6 (60°) sector model was employed. The mesh partition used in this analysis is shown in Fig. 9. The total number of meshes is 220649. The following temperature and pressure monitor points were set besides the thermocouple tree part that had been previously described. The temperature monitor points are shown in Fig. 10. Three points (T\_top, T\_Center, T\_Bottom) at the edge of the horizontal pipe of equal height to the R/V exit, one point (T\_2100) in the center of the vertical piping and one point (T\_Outlet) in the center of the top horizontal piping. T\_Outlet is set at 500mm distance from the elbow piping downstream. T\_Outlet is set in this position to rationalize the calculation, although the actual measurement point was further downstream. The R/V exit temperature for comparison with the test data was calculated taking the delay time of the flow into consideration. The pressure monitor points assigned in each flow hole as shown in Fig. 11. There are two measurement points at the inside and outside of the inner barrel on the axis of each flow hole.

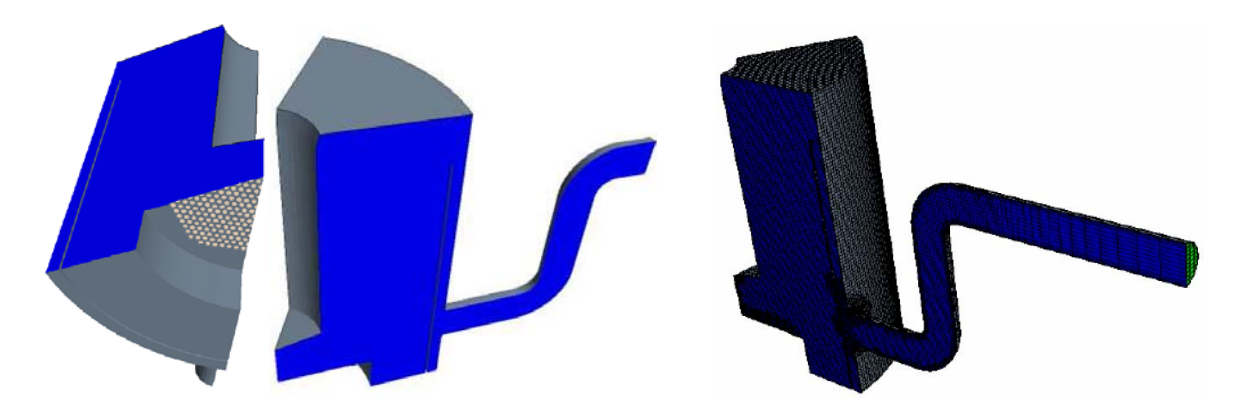


Fig. 8 The geometry for the STAR-CCM+ calculation

Fig. 9 The mesh partition

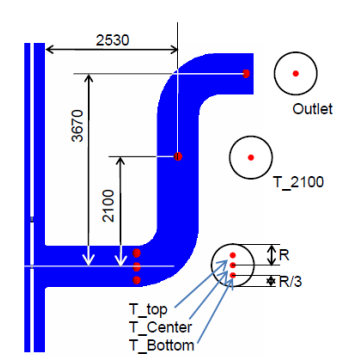


Fig. 10 Temperature measurement points

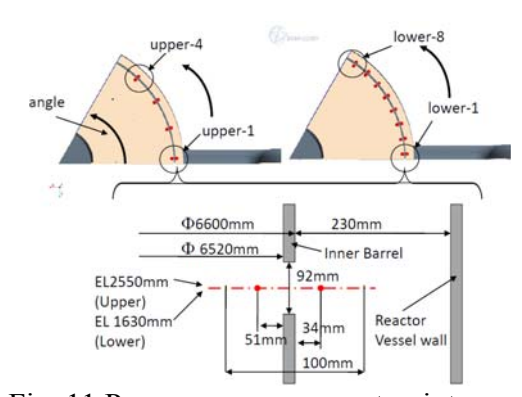


Fig. 11 Pressure measurement points

## 4. The flow pattern and temperature distribution at the steady state

Figure 12 shows the flow patterns and temperature distribution under the steady state condition. The main stream at the upper part of the core is the flow in the upward oblique direction. A large circulation flow with a rising flow along the inner barrel and downward flow along the UCS at the upper part of this main stream is observed. Downward flows along the inner barrel are formed at the lower part of this upward main stream. Low temperature sodium from the blanket fuel and the removable shielding channel flow into the concave space at the side of the core barrel and the downward flow results in temperature stratification. These characteristics are observed in both calculations.

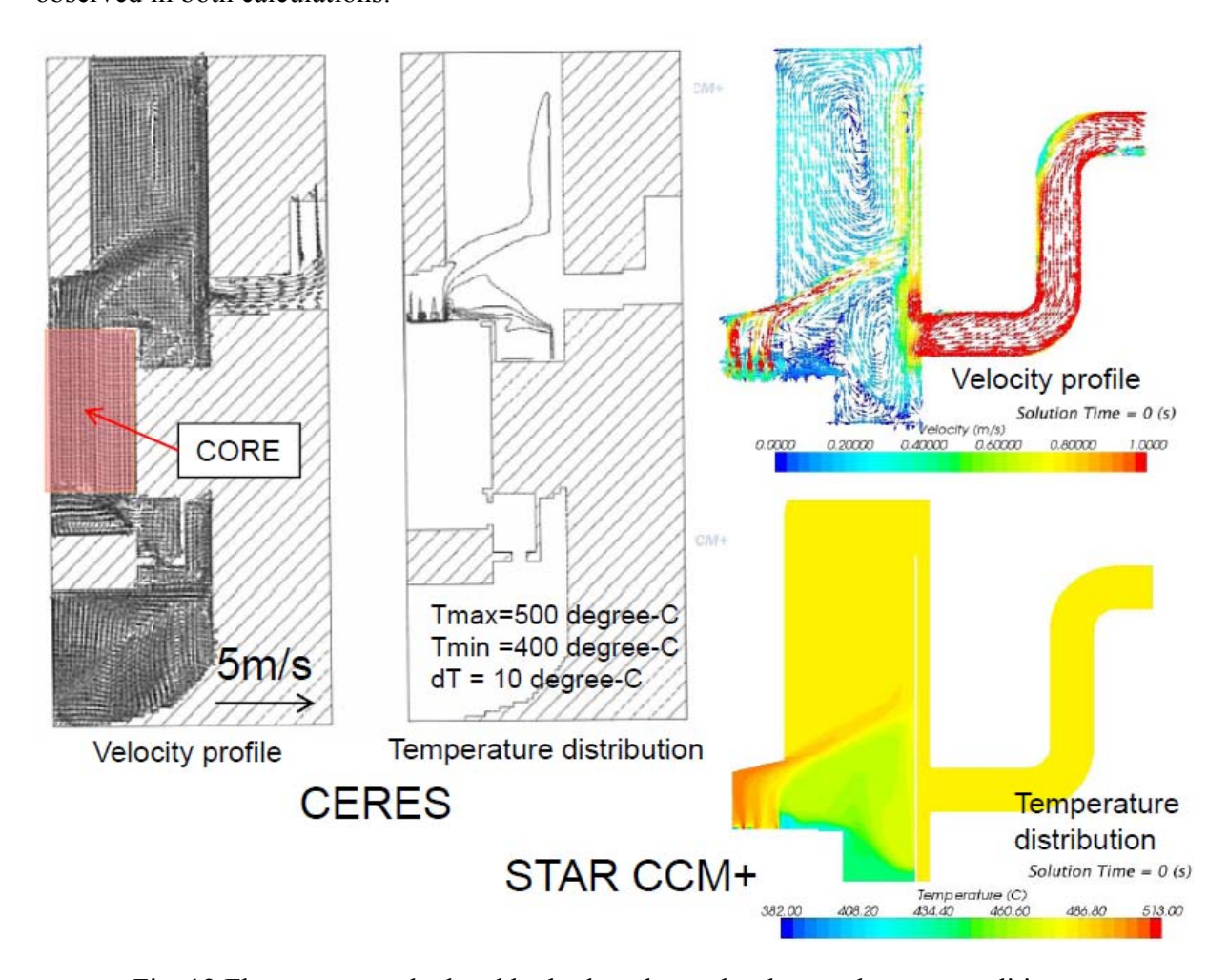


Fig. 12 Flow pattern calculated by both codes under the steady state condition

# 5. Transient calculation

## 5.1 Pressure loss coefficient

Pressure distributions along the axis of each flow hole of the inner barrel (Red dotted line in Fig. 11) under the steady state condition are shown in Figs. 13 and 14. To obtain the differential pressure of both ends of the flow hole, the required distance from the wall to ensure the pressure gradient remains constant has to be determined. Each distance is 51mm (inside) and 34mm (outside) as shown in Fig. 11. These distances are adopted as the typical pressure point of the first mesh close to the wall in the plenum model of the CERES code.

The pressure loss coefficients derived from the differential pressure obtained by the transient calculation are shown in Figures 15 and 16. These values fluctuate significantly in the initial stage of the transition, which is considered attributable to the considerable change in the velocity field near the flow holes in this stage. However, the flow stabilizes 200sec after the transient starts, and the pressure loss coefficient becomes constant. The average value of the upper flow holes was 1.88, and that of the lower flow holes was 1.94 at a stable condition.

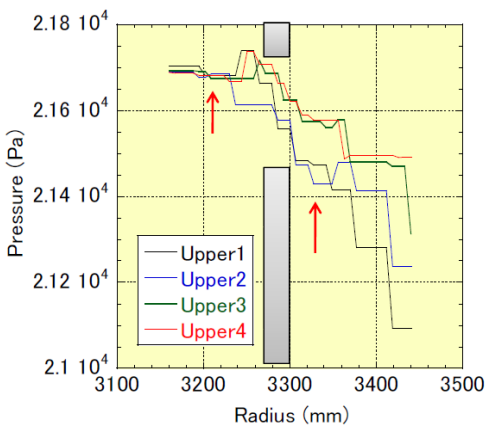


Fig. 13 Pressure distribution (Upper)

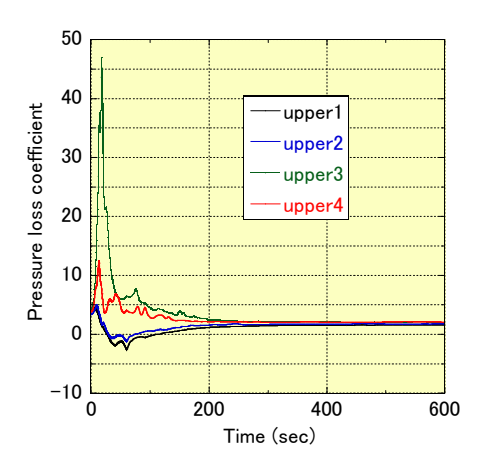


Fig. 15 Pressure loss coefficient (Upper)

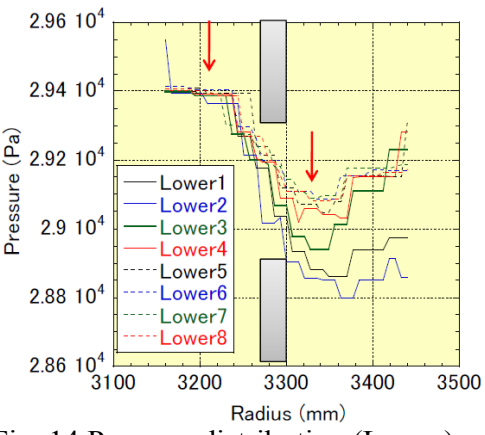


Fig. 14 Pressure distribution (Lower)

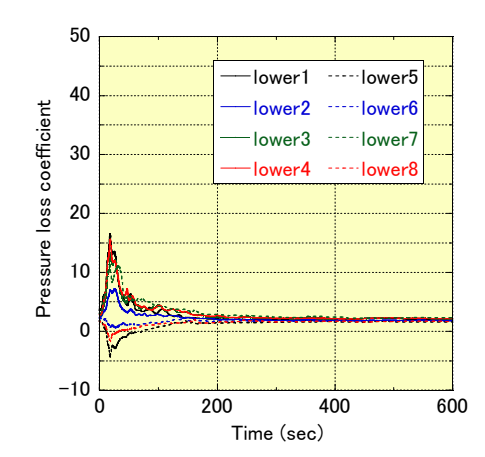


Fig. 16 Pressure loss coefficient (Lower)

Actually, the flow through the flow hole is not provided for this differential pressure alone, because of the existence of a multi-dimensional flow near the flow hole. In that sense, the pressure loss coefficients derived from these differential pressures must be considered an apparent value. The values at steady state condition were 3.75 (upper) and 2.45 (lower). The data concerning the pressure loss coefficient, conforming to the flow field having emerged and containing the flow through the flow hole, is significant in the simplified analysis.

# 5.2 Vertical temperature distribution and the flow pattern in the upper plenum

Figure 17 shows the temperature distribution along the thermo-couple tree in the upper plenum. Under a steady state condition, the temperature distribution is almost constant except for the data at the lowest elevation. This tendency can be calculated by both codes. After the plant trip starts, the temperature of the lower position in the upper plenum decreases as the core outlet temperature decreases. The temperature stratification is generated in the plenum because originally hot sodium existed in the upper plenum, and the boundary rises over time. It is found that the change in the thermal stratification can be effectively simulated well during transient by both codes. Because the pumping of high temperature sodium to the liquid surface in R/V was maintained until 1200 seconds after the reactor trip, a tendency for the high temperature to continue in the upper position surfaced in the test data. Because this pumping is not modeled in both codes, the tendency at the upper part is not especially discussed here. As for the analytical result of the CERES, the rising speed on the stratification field side is slightly slower compared with the STAR-CCM +.

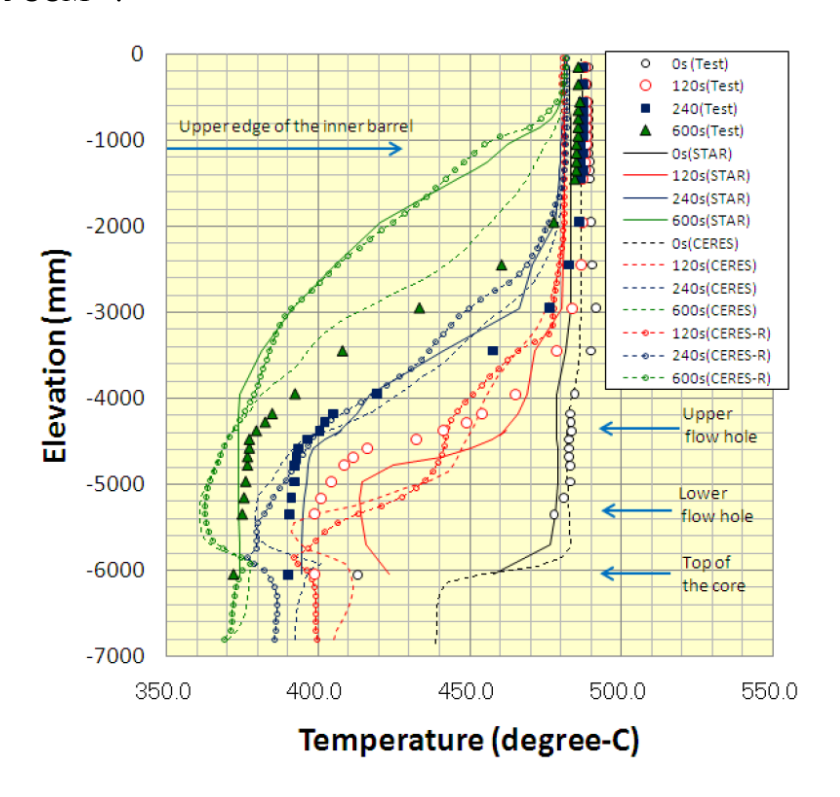


Fig. 17 Vertical temperature distribution

Figure 18 shows the changing of the flow pattern by flow streams in the upper plenum during the transient calculated by the STAR-CCM+ code. From the figure, it is found that the temperature of the reactor core outlet sodium decreases and the sodium that flows upstream also does so over time. The low temperature sodium escaping via flow holes and the high temperature sodium that flows down in the annulus part is mixed, and enters the R/V exit piping.

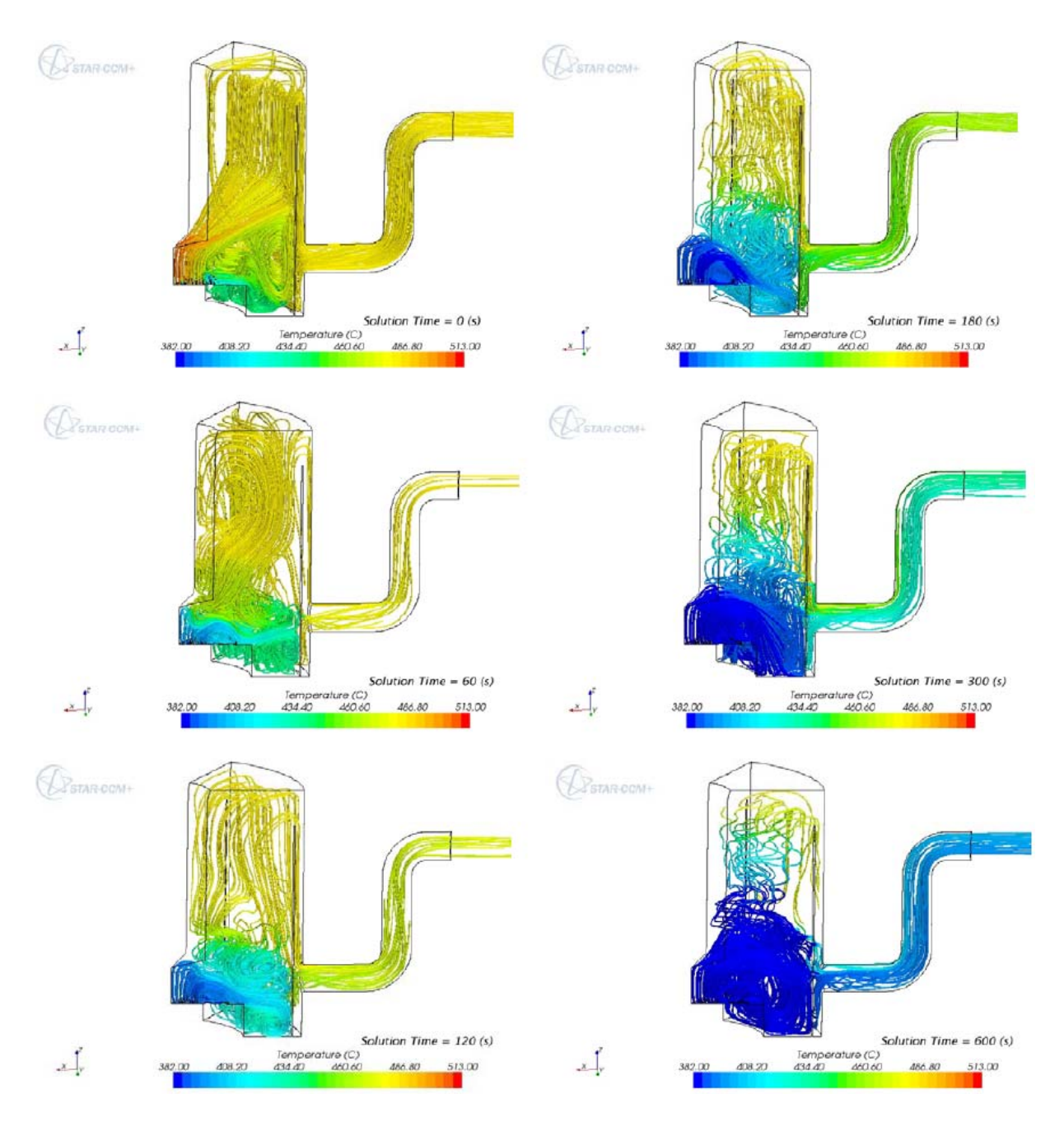


Fig. 18 Flow pattern changing during transient

## 5.3 Flow path and the R/V outlet temperature

Temperatures at the monitor points are shown in Fig. 19. T\_Center, T\_top and T\_Bottom are almost the same until 200 sec after the reactor trip, however, the T\_top indicates a higher value than other points after 200 sec. This is thought to be attributable to insufficient mixing of the high temperature sodium that flows down from the upper part of the plenum through the annulus part and enters the exit piping, due to the stability of the velocity field. The temperature distribution in this piping can also be confirmed in Fig. 18. However, it seems that this temperature distribution is roughly canceled out via two elbows.

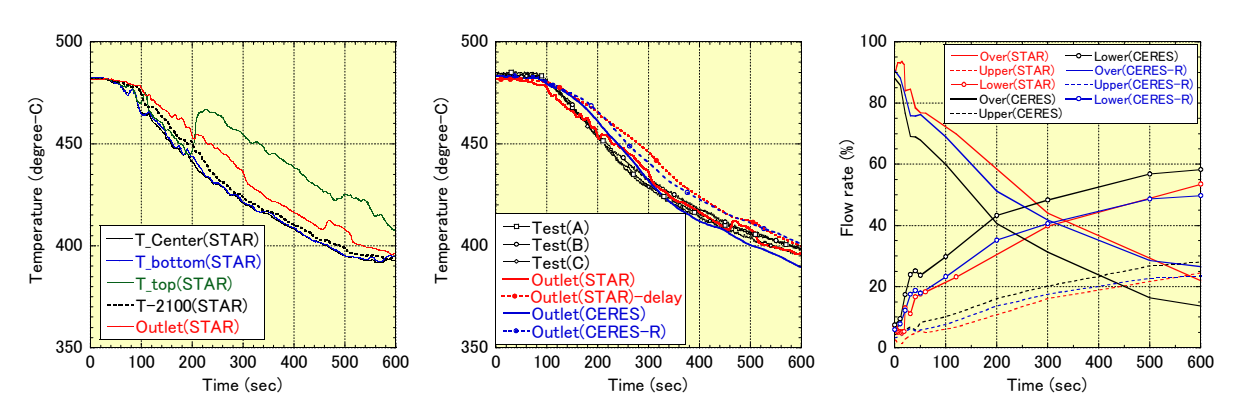


Fig. 19 Monitor point Temperature

Fig. 20 R/V outlet Temperature

Fig. 21 Flow distribution

Figure 20 shows a comparison of the R/V outlet temperatures. Based on the result of the analysis, the transportation delay to the thermocouple position is considered [4]. Both the temperature of the raw result and that taking the delay time by STAR-CCM + calculation into consideration are shown as examples. As for the CERES result, it is understood that the temperature drop is swift compared with the test result. Conversely, the result of the STAR-CCM+ is almost the same as the test result [5] for the speed of the temperature drop. The sodium that flows from the core reaches the R/V exit piping through three flow paths: the gap between the inner barrel top and the liquid surface, the upper flow-holes and the lower flow-holes respectively. Figure 21 shows the computational result of the ratio of flow distribution. It is found that the ratio of flow through the flow hole is large in CERES compared with the STAR-CCM+. Because sodium from the flow hole was at a comparatively low temperature, the R/V outlet temperature became the result of the early decrease. The low flow rate for the upper part of the upper plenum also leads to a slower speed on stratification rising of axial temperature in CERES.

### 5.4 Revised calculation by the CERES code

Because new pressure loss coefficients of the flow holes have been proposed by analyzing STAR-CCM+, the revision analysis of CERES (called CERES-R) that used those values was performed. Figure 17 also shows the result of CERES-R. It is found that the rising speed of the stratification boundary exceeds that of the CERES original analysis. The axial temperature distribution of CERES-R, particularly at the time of 600sec, is very close to the result by the STAR-CCM+. Fig. 21 also shows the flow distribution of the CERES-R. It is found that the

results of the CERES-R resemble those of STAR-CCM + in terms of flow distribution and the R/V outlet temperature of CERES-R reaches a value close to the change speed of the test. Based on these results, it was clarified that similar results that resemble a detailed multi-dimensional thermal hydraulic analysis code can be obtained by the plenum model of the CERES code when appropriate parameters such as a pressure loss coefficient can be applied. Moreover, it has been understood that the sensitivity of the flow hole loss coefficient is considerable when the upper plenum of MONJU is analyzed by the plant dynamic analysis code based on the flow network model.

#### 6. Conclusion

The plant trip test of the MONJU was analyzed by general-purpose multi-dimensional thermal hydraulic analysis code STAR-CCM+ and the plant dynamic analysis code CERES, and the following findings were obtained:

- (1) Because the low temperature sodium flows out from the core, the thermal stratification is observed against the hot sodium that existed in the upper plenum during the transient. The rising speed on the stratification boundary obtained by CERES original analysis was slower than the result of STAR-CCM+.
- (2) The flow pattern during the MONJU trip test was clarified from the analysis of STAR-CCM+. The R/V outlet temperature of the MONJU was influenced from the flow distribution of the flow holes. The pressure drop coefficient of the flow holes that led to the analysis by the flow network code etc. was derived from the analysis of STAR-CCM+.
- (3) The revision analysis by the CERES code that used the obtained pressure loss coefficients showed results almost similar to STAR-CCM+. Based on these results, the performance of the plenum model of the CERES code was confirmed.

#### 7. References

- [1] F. E. Dunn, F. G. Prohammer, D. P. Weber, and R. B. Vilim, "The SASSYS-1 LMFBR SYSTEMS ANALYSIS CODE", <u>Proc. of the Int. Topical Meeting on FAST REACTOR SAFETY</u>, Vol.2, pp.999-1006, Knoxviile, Tennessee, April 21-25, 1985
- [2] Y. Nishi, N. Ueda, I. Kinoshita, and E. Greenspan, "Computational Analysis of the Thermal-hydraulic Characteristics of the Encapsulated Nuclear Heat Source", <u>Nuclear Technology</u>, Vol.152, DEC.2005.
- [3] Y. Nishi, N. Ueda, S. Nishimura, T. H. Fanning and F. E. Dunn, "Verification of the plant dynamics analytical code CERES; Comparison with EBR-II Tests", <u>Proc. of the ICAPP' 10</u>, Paper 10271, San Diego, CA, USA, June 13-17, 2010
- [4] A. Ohtaki, A. Miyakawa and S. Nakai, "Development of dynamic analysis code Super-COPD Validation by MONJU functional test-", <u>PNC TN9410 95-060</u>, 1995 (in Japanese).
- [5] Y. Nishi, N. Ueda, I. Kinoshita, A. Miyakawa and M. Kato, "Verification of the plant dynamics calculation code CERES using the results of the plant trip test of prototype fast breeder reactor "MONJU"", JNC TY2400 2005-001, 2005 (in Japanese)